RESONANT EXTRACTION OF THE PROTON BEAM FROM THE DUBNA SYNCHROPHASOTRON

I.B.Issinsky, E.M.Kulakova, V.N.Lysyakov,
K.P.Myznikov x), N.I.Pavlov, N.M.Tarakanov x) and
L.P.Zinoviev

Laboratory of High Energies,
Joint Institute for Nuclear Research,
Dubna, USSR

June, 1967

1. Introduction

The advantages achieved by using the radial free oscillation resonance for jumping the beam onto the extracting magnet allowed to choose this method for the proton beam extraction from the Dubna synchrophasotron [1]. The most important advantage is that in exciting the $\nu_R = 1/2$ resonance applied in the accelerator particles are bunched according to free oscillation phases at one particular azimuth. This means that particles enter the gap of the beam extracting magnet or the septum-magnet with small angular divergence. Thus, it is possible rather simply to eliminate difficulties due to the extracted beam focusing when it passes the accelerator fringing field. The problem is also simplified by the fact that the beam at the end of acceleration has a very small energy spread (1-2 MeV at 10 GeV). Therefore, there is no necessity to employ the achromatic system compensating dispersion. On the other hand, the $\nu_R = 1/2$ resonance provides the fast free oscillation build-up. This allows to extract the beam for 30- 100 μsec. [2,3].

2. Method

The solution of the problem of fast proton beam extraction by using the half- integral resonance consists in

1) resonance build-up of free radial oscillations and protons jump into the gap of the septum-magnet;

2) deflection and focusing in the septum-magnet and the accelerator quadrant;

3) extracted beam transport.

Fig.1 shows schematically the extraction and the main equipment lay-out. The change in the field index n is introduced in accelerator quadrants I and II. There is a beam deflecting magnet in the straight section between quadrants II and III. After being deflected in this magnet the beam passes quadrant III and emerges from the vacuum chamber. The first stage of the transport system deflects the beam by $\sim 6^\circ$ and produces the first stigmatic image. Proton motion with the half-integral resonance was calculated with the computer using the exact motion equations, the real magnetic field distribution corresponding to the proton energy of 10 GeV and with the account of the accelerator structure. Resonant conditions were produced in the synchrophasotron by identically varying with time the field index n in accelerator quadrants I and II. Motion for 60 protons was calculated with various initial amplitudes and phases radial free oscillations. The character of the beam jump onto the septum-magnet was considered with various perturbation value Δn and various magnet positions with respect to the central orbit. The angles of particle entrance into the magnet are decreased with increasing the jump depth (Fig.2) and increasing the turn number at which particles get into the gap (Fig.3). The turn number is counted from the moment of perturbation increment start. Proton trajectories in septum-magnet and accelerator quadrant were computed also using the exact equations of charged particle motion in the magnetic field by numerical integration [4]. Field distribution in the accelerator median plane was described in the form of Tables compiled on the results of magnetic measurements of 1965 [5]. Since the accuracy of measurements was $\pm 0.3\%$, the field components were determined up to the second-order terms. The field in the septum-magnet was given analytically. Fig.4 shows beam distribution at the end of the quadrant III in the horizontal plane, the septum-magnet field being uniform. It is evident that due to the defocusing effect of the accelerator fringing field the beam is not acceptable for further transport. If gradient focusing ($n < 0$) is used in the septum-magnet due to the combined effect of the magnet and the accelerator fringing field the beam can be focused in both the planes. Its horizontal dimension is considerably reduced in this case.

---

x) Now working at the Institute of High Energy Physics (Serpukhov).

However, when the angle of deflect in the septum-magnet is increased, the horizontal size of the beam is also increased due to the effect of the fringing field which cannot be compensated by means of gradient in the septum-magnet. The angle of deflect and the gradient in the septum-magnet were choosen so that the emerging beam had the minimal horizontal size and after the bend in the first stage of the transport system passed by the magnet yoke of quadrant IY. The dependence of vertical and horizontal dimensions of the emerging beam core upon n for the chosen angle of deflect is given in Fig.5. In the optimum case the deflecting angle was 55°20'' and n = -75. Since there is the dependence of the particle angle at the entrance into the magnet upon time, additional focusing of the beam can be obtained in the horizontal plane, producing the septum-magnet field varying with time. Fig.6 shows for comparison the beam distribution in the horizontal plane for the angle of deflection 55°20 '' and n = -75 and the time-constant field (a) and field decreasing at a rate of 2.95 Gauss/turn (b).

When calculating proton motion in the septum-magnet the non-linear effect of the second order were taken into account [6]. The field configuration was found for the septum-magnet which reduced the nonlinear effect to the minimum

$$B_z\,(R_{os}+\rho\,,z) = B_o\left[1-n\frac{\rho}{R_{os}}+\frac{n}{2}\left(\frac{\rho}{R_{os}}\right)^2\right], \qquad (1)$$

$$B_R\,(R_{os}+\rho\,,z) = B_o\frac{nz}{R_{os}}\left(-1+\frac{\rho}{R_{os}}\right).$$

Here B_o is the field in the septum-magnet at the orbit of the equilibrium radius R_{os};

ρ is displacement from the equilibrium radius;

z is displacement from the magnet median plane;

n is given at equilibrium radius R_{os}.

3. Extraction System Equipment

Resonant conditions in the accelerator are achieved with the help of windings in the first and second quadrants located on the upper and lower magnet poles. Current pulse of a 340 A amplitude gives $\Delta n = 0.22$ [2] in the windings at 10 GeV.

The parameters and the septum-magnet design depend upon the requirements of the calculational and experimental character in Sections 2 and 4. The magnet gap variable in height has the form described by the equation

$$d = d_o \Big/ \left[1 - n\frac{\rho}{R_{os}} + \frac{n}{2}\left(\frac{\rho}{R_{os}}\right)^2\right] \qquad (2)$$

obtained basing on (1) and under the assumption that $\mu = \infty$. Here d_o is the gap height at the equilibrium radius R_{os}. The magnet aperture is chosen basing on the particle density distribution for particles at the entrance in the gap (Fig.11 and 12). In this case d_o = 44 mm, the transversal dimension of the aperture is 120 mm. The magnet yoke consists of insulated E-330 steel sheets 0.35 mm thick. The magnet iron is 620 mm long. The maximum field at the equilibrium radius is 0.948 Wb/m^2. The magnet weight is about 300 kg.

According to the considerations risen by the supply system, the magnet winding has 14 coils. Its mechanical and electrical strengths determine the septum thickness which is 10 mm. Small duty factor of pulses ($1:3.10^{-4}$) allows one to avoid forced cooling. There are windings on the magnet poles which regulate the magnetic field gradient.

The general view of the septum-magnet is shown in Fig.7. When in the working position, the magnet is 200 mm apart from the accelerator central radius. It is moved vertically by means of a compact hydraulic mechanism (Fig.8) for 0.8 sec. The working stroke of the mechanism is 250 mm.

The magnet winding is supplied by a discharge of the capacitor bank by means of the thyratrons. Half sine wave current pulse has duration 3 m sec.

Fig.9 shows the dependence of the amplitude magnetic field value in the septum-magnet median plane for B_o = 0.76 Wb/m^2 obtained with a Hall probe at various currents in the gradient winding.

Since at fast extraction the particles pass the fringing field in front of the septum not more than once there are no essential distortions. Therefore, no special efforts were taken to reduce the fringing field.

4. Experimental Results

In order to choose the optimum dimensions of the septum-magnet gap the preliminary experimental investigations of particle hitting on the target were carried out in resonant conditions at 10 GeV [1].

With this aim nuclear emulsion was placed inside the synchrophasotron chamber at the coordinates corresponding to the position of the septum-magnet. The emulsion was introduced into the chamber by the end of the acceleration cycle using a plunging target. After that the current pulse was sent to the winding of the re-

sonance excitation and the beam was hitted the emulsion. Conditions were made in which multiple passage of particles through emulsion was excluded.

Fig.10 shows particle hitting on the emulsion for the optimuj case when its edge is +200 mm from the chamber center, acceleration occurred at the central orbit and the excitation was 0.22. The results of measurements of intensity distribution on emulsion in the radius direction are shown in Fig.11. In the histogram the number of particles entered the interval 5 mm wide related to the total number of particles hit the emulsion is at the ordinate axes. This case is optimal from the point of view of the jumping depth and the loss at the septum. This coincides with caloulation results. Fig. 12 shows the relative distribution of intensity along the vertical 1 cm apart from the emulsion edge. The distribution was taken also for the optimum case.

Basing on the distribution obtained one can estimate particle loss on the septum. Taking into account some small loss in the magnet aperture the efficiency of the extracted beam at the entrance in the exit window should be $\sim$ 80% of the circulating beam.

The first experiments on proton extraction were performed at 7.5 GeV. The extracted beam was turned with a scintillation probe placed in front of the beam exit from the accelerator chamber (64^{o} from the begining of quadrant III). The probe is a 4x4x10 mm^3 plastics fastened to the thin holder. There is an optical system with a photomultiplier. The probe was moved remotely along the radius and the vertical. Fig. 13 shows the radial and vertical distribution of the beam at this azimuth with various n in the septum-magnet. The distribution was taken during several pulses. Therefore, the obtained beam dimensions were overestimated due to the instability of its position. Fig.14 shows for comparison the beam vertical distribution with emulsion irradiation by one pulse at the same azimuth. At the vacuum chamber exit the beam was detected in nuclear emulsions. A TV system was used in tuning and observation. The preliminary efficiency measurements made with nuclear emulsion in conditions differing from optimal give 50%. Suggestions are made to increase the efficiency by changing the multiturn winding for a single turn one with the septum thickness 3.8 mm and the careful tuning of the optimal resonant conditions in beam hitting into the magnet gap.

The first stage of the transport system gives the stigmatic image within the accelerator housing. This bending-focusing system consists of the two gradient magnets (n=-140) and the two quadrupole lenses with the same gradient sign.

Fig.15 shows the passage of the extreme trajectory through the parts of the first stage of ion-optical system in the horizontal (a) and vertical (b) planes.

We wish to thank the many members of Ejection Group S.A. Novikov, W.S.Mironov, W.A.Shurchovezky, W.N.Buldakowsky, J.F.Kusagin, A.I.Kryukov, M.D.Ershov, E.I.Objesdnov who contributed their efforts. W.I.Kotov, L.A.Smirnova, N.N.Govorun, B.W.Wasilishin for the help in calculations; the Electroradio Group under J.A.Bychkov, W.M.Nechaev for the help in constructing of the magnet M_2.

References:

1. L.P.Zinoviev, I.B.Issinsky, E.M.Kulakova, K.P.Myznikov, N.I. Pavlov, Proc. Int.Conf. on High Energy Accelerators, Dubna, 1963.
2. L.P.Zinoviev, I.B.Issinsky, V.I.Kotov, E.M.Kulakova, K.P.Myznikov, N.I.Pavlov, Preprint P- 2387, Dubna, 1965.
3. L.P.Zinoviev, N.B.Issinsky, V.I.Kotov, E.M.Kulakova, K.P.Myznikov, N.I.Pavlov, Preprint 1939, Dubna, 1963. PTE No.1, 33 (1965).
4. E.M.Kulakova, K.P.Myznikov, L.A.Smirnova, B.V.Feoktistov, Preprint P-2880, Dubna, 1966.
5. E.A.Dementyev, I.B.Issinsky, E.M.Kulakova, K.P.Myznikov, M.Polak, F.Hovanets. Preprint P- 2818, Dubna, 1966.
6. I.B.Issinsky, V.I.Kotov, E.M.Kulakova, K.P.Myznikov, L.A.Smirnova, Preprint 2326, 1965. Nuclear Instr. and Meth. 48 (1967) 147-150.

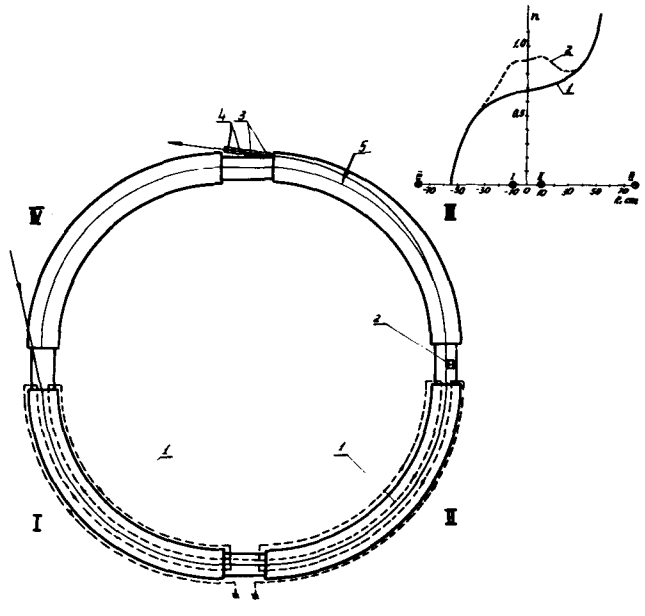

Fig.1. The lay-out for fast beam extraction.

1. Excitation windings.
2. Septum-magnet M_1 with the hydraulic system.
3. Beam-bending magnet M_2.
4. Lenses of the transport system.
5. Probe.

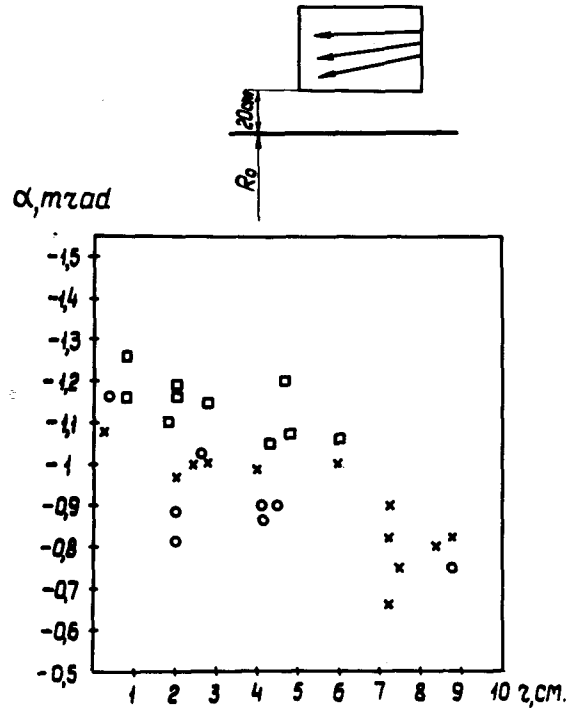

Fig.2. Particle angles at the entrance into the septum-magnet vs the jump depth into the gap when the magnet edge is R_o + 20 cm and A n = 0.22.

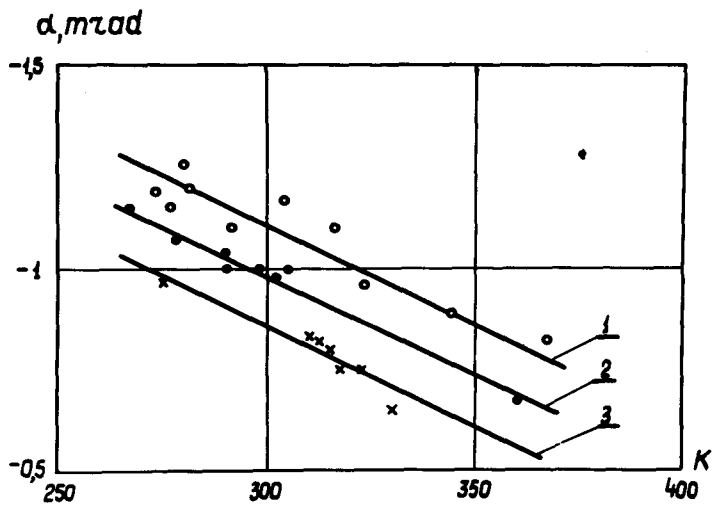

Fig.3. Particle angles at the entrance into the magnet vs the turn number. Line I corresponds to particles entering the gap at the distance of 20÷22 cm from the central region, line 2 is 22÷24 cm, line 3 is 26÷30 cm.

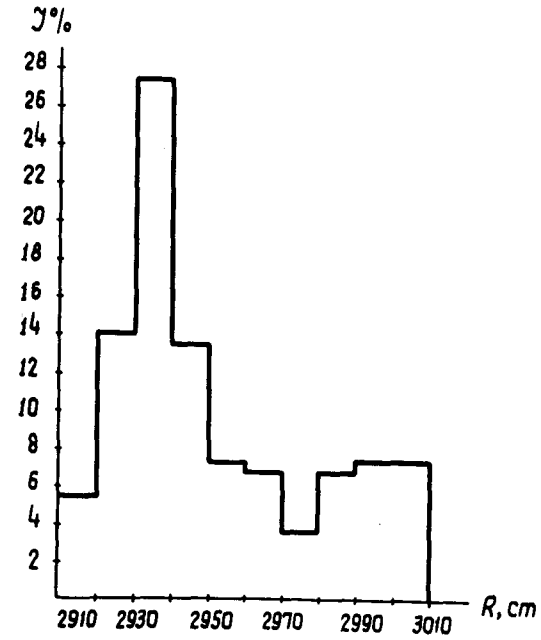

Fig.4. Extracted beam intensity distribution at the end of the quadrant III in the horizontal plane with the uniform field in the septum-magnet.

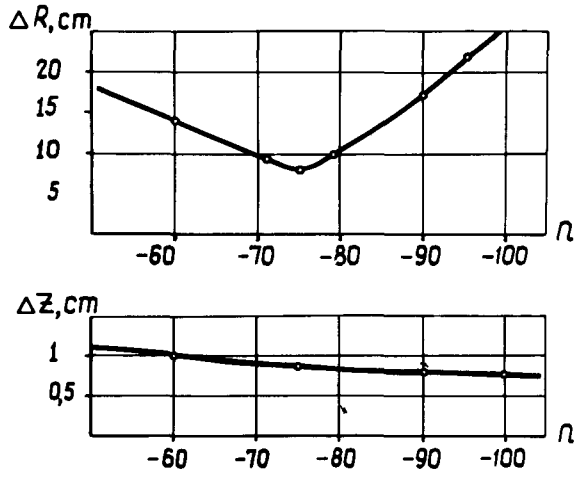

Fig.5. Size of the extracted beam core in the horizontal and vertical planes vs n in the septum-magnet at the angle of bend $\beta_0 = 55°20''$.

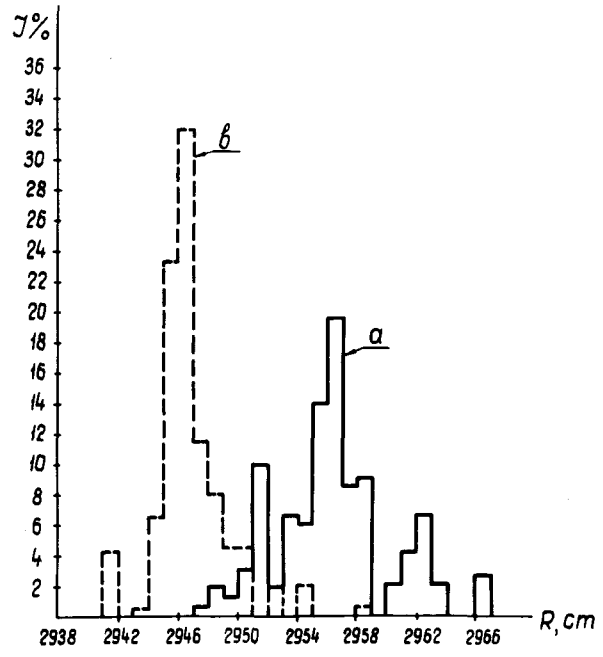

Fig.6. The intensity distribution of the extracted beam in the horizontal plane with $\beta_0 = 55°20''$, n = -75.
a) the field is changed with time,
b) field is decreased with time at 2.95 Gauss/turn.

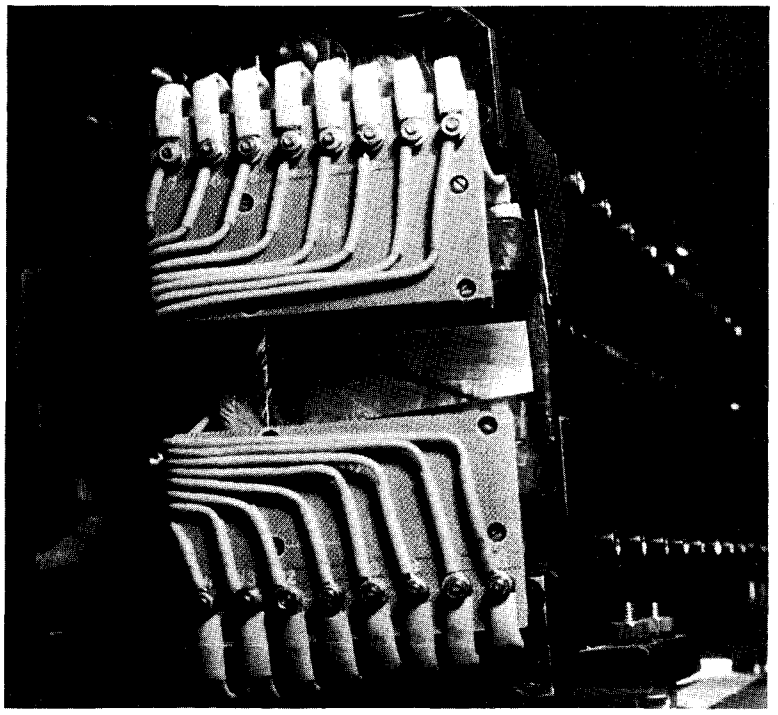

Fig.7. General view of the septum-magnet.

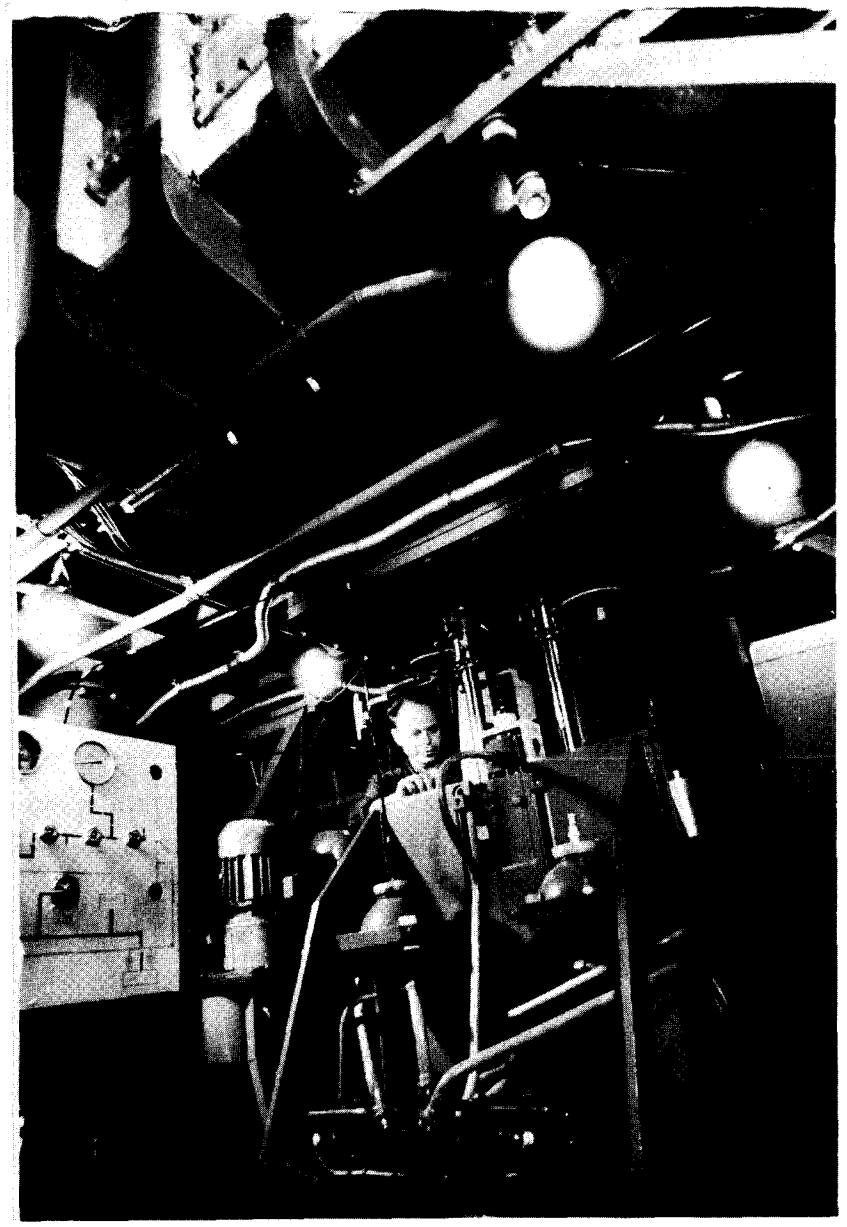

Fig.8. The hydraulic mechanism.

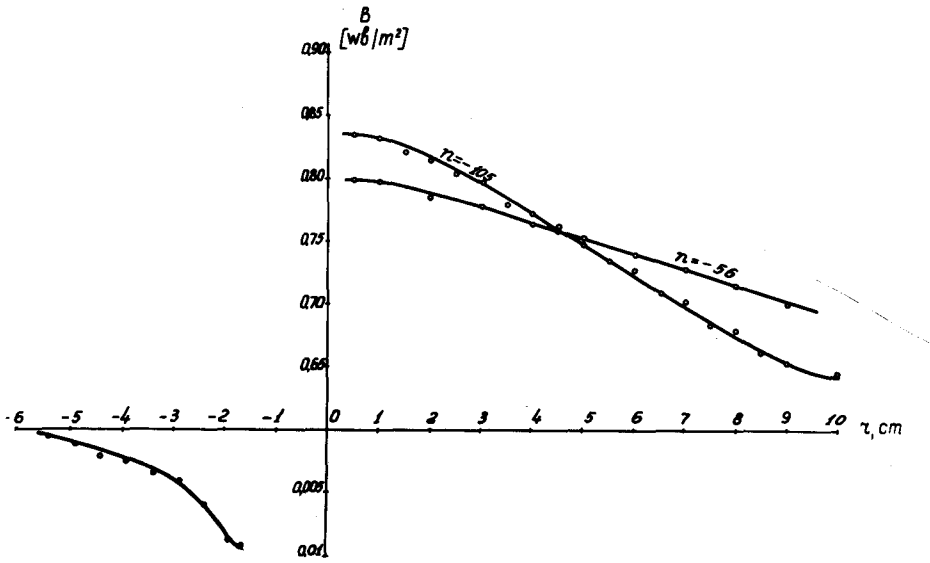

Fig.9. Magnetic field amplitude in the septum-magnet vs various n.

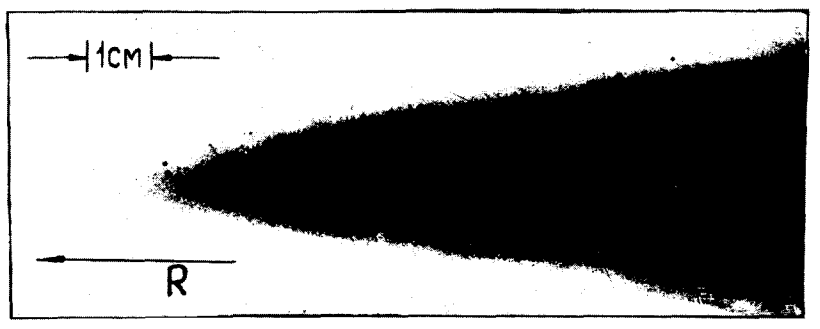

Fig.10. Beam jump to emulsion with $\Delta n = 0.22$ and $R_o + 20$ cm.

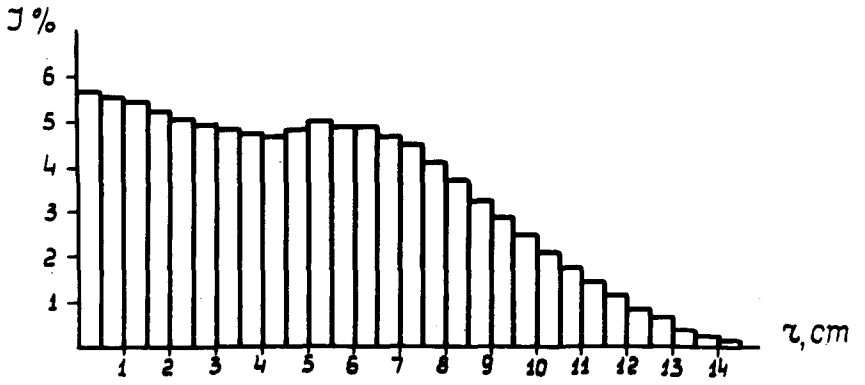

Fig.11. Intensity distribution on emulsion along the radius with $\Delta n = 0.22$.

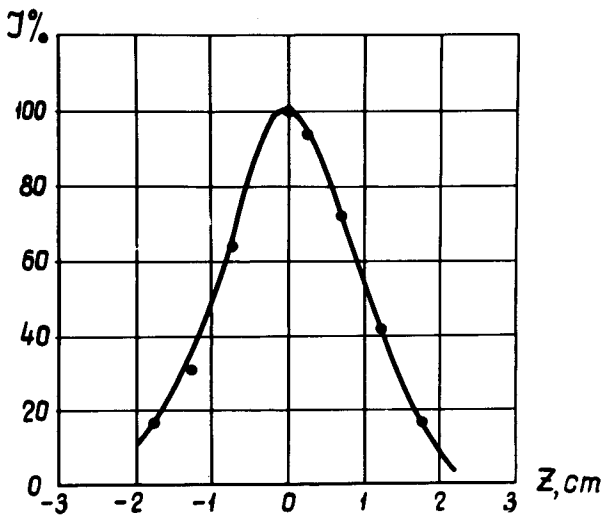

Fig.12. Intensity distribution on emulsion along the vertical with $\Delta n = 0.22$.

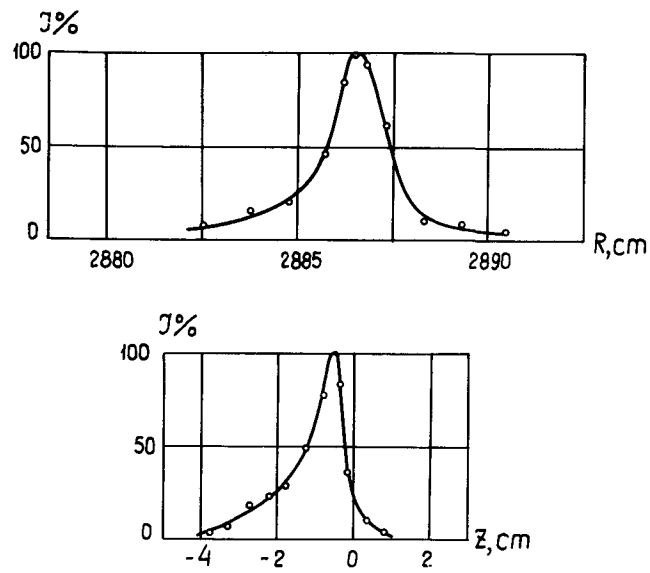

Fig.13. Beam distribution along the radius and the vertical taken with a probe at the end of quadrant III, n = -40 (curve 1), n = -36 (curves 2 and 4), n = -33 (curve 3).

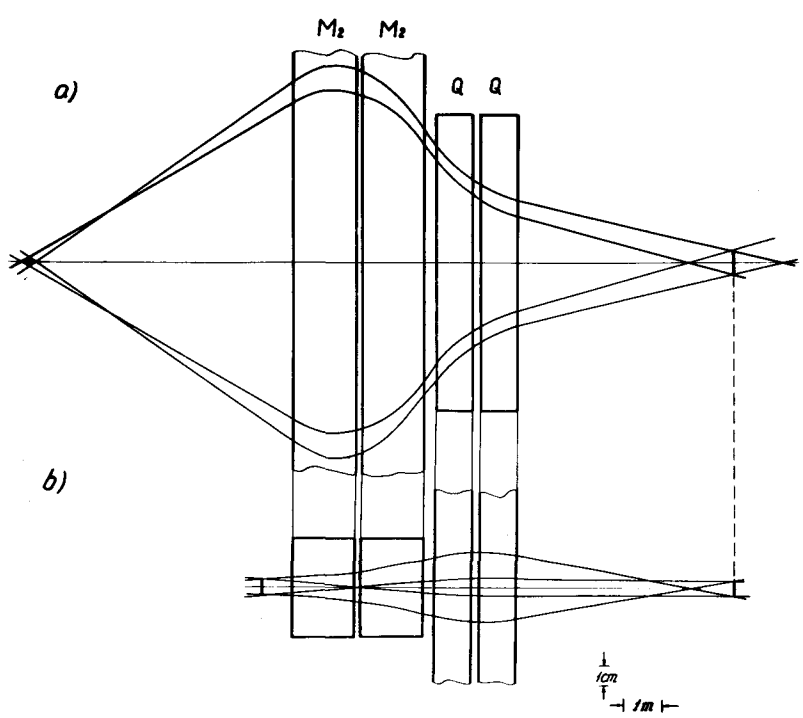

Fig.15. Passage of extreme trajectories through the first stage of the ion-optical system in the horizontal (a) and vertical (b) planes.